Defense Technical Information Center
Compilation Part Notice

ADP012085

TITLE: Supercavities in Compressible Fluid

DISTRIBUTION: Approved for public release, distribution unlimited

This paper is part of the following report:

TITLE: Supercavitating Flows [les Ecoulements supercavitants]

To order the complete compilation report, use: ADA400728

The component part is provided here to allow users access to individually authored sections of proceedings, annals, symposia, etc. However, the component should be considered within the context of the overall compilation report and not as a stand-alone technical report.

The following component part numbers comprise the compilation report:
ADP012072 thru ADP012091

Supercavities in Compressible Fluid

A. D. Vasin

State SRC TsAGI, Moscow, Russia
17, Radio str., Moscow, Russia

Summary

The basic results obtained by the author in the theory of supercavities in compressible fluid have been presented. Some peculiarities of the theoretical methods application for the supersonic flows and their difference from the analogous flows in air have been noted. The basic correlations for the shock waves in the water are considered.

Axissymetric supercavities in sub- and supersonic compressible fluid have been researched using the asymptotic method. An integro-differential equation for the cavity profile was deduced. The outer solution was found and for the thin cone-cavitators the solution was obtained for the whole area of the flow.

Based of the modern numerical methods the algorithm of calculation of axisymmetric cavities in sub- and supersonic compressible fluid flow has been worked out. The results of calculation of axysimmetric supercavities downstream of a disk within the range of the Mach numbers $0 \leq M \leq 1.4$ have been represented. As a result of the analysis for the different Mach numbers the following was defined: the cavitation number, the cavitation drag ratio, the mid-section radius, the cavity shape, the distance of shock wave from a disk (for supersonic flow). The conical flows in a supersonic water stream have been calculated by the numerical method.

The results obtained by the author have been compared with the known experimental and theoretical results of other investigations.

Introduction

The axisymmetric and three-dimensional supercavities in incompressible fluid have been intensively studied since the early 1950's. A large amount of works have been published on three-dimensional supercavities in incompressible fluid. There were about several hundred of them. It should be noted that there have been a few publications on the three-dimensional supercavities in a compressible fluid (in contrast to the case of incompressible fluid). This situation is a result of both the absence of practical interest to this problem before 1980 and the complexity of the problem itself. The only work was Gurevich's work [1] that was published in 1947. In this work the expansion law for a cavity downstream of a body was examined for zero cavitation number and generalized to include the subsonic case.

Since the early 1980's in the USSR and in the USA the interest in supercavities in a compressible fluid has increased. The necessity to come up with the supercavities theory in a compressible fluid appeared. The following works have been made based on the slender body theory. These are the works: Yakimov [2,3], the author [4,5] and Serebryakov [6,7]. On the basis of the early numerical method Al'ev [8] has calculated the cavity past a thin cone. The theoretical investigations on two-dimensional supercavities in compressible fluid were carried out by Nishiyama [9].

The slender body theory has a limited application for calculation of supercavities in compressible fluid. For blunt cavitators such as a dusk or a blunt cone, this theory does not provide a way to obtain the complete data for the cavitation flow, for example, the cavity shape immediately downstream of the cavitator, and the cavitation drag. The linear equation for the potential of compressible fluid flow past

slender axisymmetric bodies is inapplicable on the transonic velocity range. Moreover, for the case of supersonic flow the slender body theory faces some major difficulties which is shown by the author's investigations.

The recent development of the numerical methods and widespread use of computers have made it possible to calculate compressible cavitation flows efficiently. It should be noted that the numerical calculations have been carried out by Zigangareeva and Kiselev [10] and by the author [11,12].

1. The application of the slender body theory for the investigation of supercavities in subsonic flow

The case of subsonic cavitation flow past a thin cone has been considered in chapter 2 of lecture #1. The Riabouchinsky scheme has been applied (Fig. 3 in lecture #1). An integro-differential equation for the cavity profile has the form of correlation (2.6) in lecture #1. In lecture #1 we have considered the case when the parameter of the cavity thinness has the same order as the parameter of the cavitator thinness ε equal to the ratio of the cone radius to its height. For the whole area of the flow the solution has been obtained by the method of expansion into asymptotic rows (rows have the form of correlations (2.6) in lecture #1). The first approximation of the cavity profile is represented by an ellipsoid of revolution (equation (2.9) in lecture #1). The second approximation is determined from the equation which was obtained after the equalization of members at ε^4 [13].
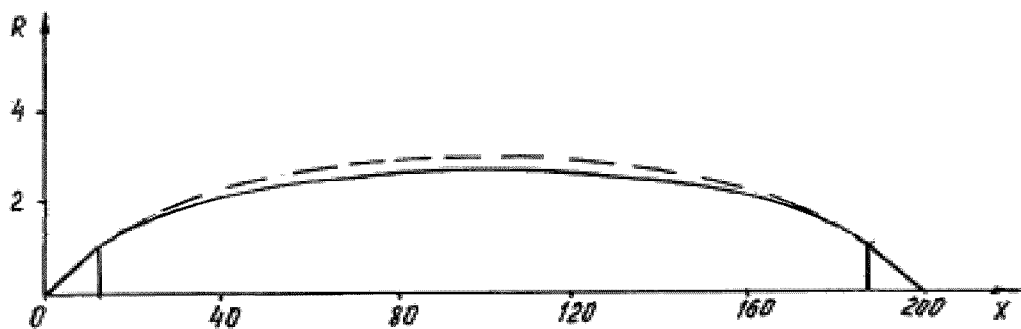

Fig. 1 **Cavity profile in subsonic flow for the cone $\alpha=5°$; the broken curve corresponds to the first approximation, the continuous curve corresponds to the second approximation**

In Fig. 1 the broken curve corresponds to the first approximation of the cavity profile $R(x)$ past the cone with the apex half-angle equal to 5°. The total length L equals 200 (the geometric dimensions are scaled by the radius of the cone base, the description of the geometric dimensions is given in chapter 2 of lecture #1). The continuous curve corresponds to the second approximation of the cavity profile. From Fig.1 it is evident that the second approximation is close to the first one, i.e. the second members of asymptotic row are smaller than the first ones.

Besides, for the cavities past the thin cones the cavitation numbers σ are determined at the different Mach numbers M ($\sigma = 2(P_0 - P_k)/\rho V_0^2$, where P_0 is the free stream pressure. P_κ is the pressure within the cavity, ρ is the fluid density, V_0 is the free stream velocity; $M=V_0/a_0$, where a_0 is the free stream speed of sound). The dependences $\sigma(M)$ are determined at the constant cavity length L_k and the total length L equal to 200.
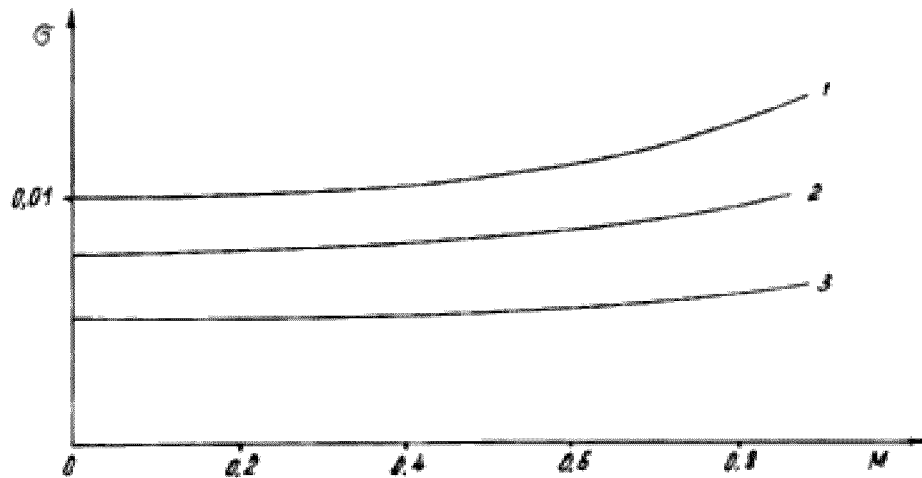
Fig. 2   Dependence of σ on M; curves 1-3 correspond to α=15°, 10° and 5°

In Fig.2 the dependences $\sigma(M)$ are shown at various cone apex half-angles α (curves 1-3 correspond to α=15°, 10° and 5° respectively). Thus, for the given cone at the constant value of L or L_k the cavitation number increases with the Mach number and the cavity profile remains invariable.

After implementation of the transformations analogous to the ones in chapter 2 of lecture 1 we can determine the expression for the pressure coefficient on the thin cone surface [13]. Integrating the pressure coefficient on the cone surface we obtain the cavitation drag coefficient C_x (normalized by the area of the cone base πR_n^2, where R_n is the radius of the cone base). In Fig. 3 the dependences $C_x(M)$ are shown at various cone apex half-angles (curves 1-3 correspond to α=15°, 10° and 5° respectively).

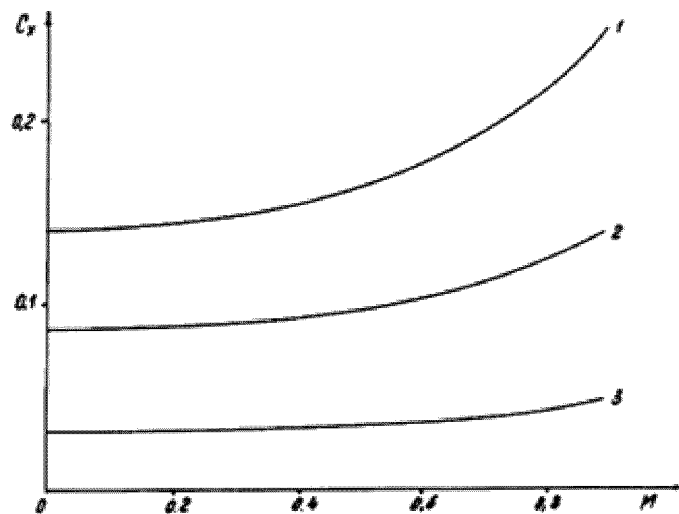**Fig. 3   Dependence C_x on M; curves 1-3 correspond to α=15°, 10°, 5°**

The character of the dependences $C_x(M)$ (Fig.3) corresponds to one of the dependences $\sigma(M)$ (Fig.2). This is a consequence of the law of conservation of momentum applied to the cavity middle-section plane. The law of conservation of momentum can be written in the following form [14]

$$R_k = \sqrt{\frac{C_x}{k\sigma}} \qquad (1.1)$$

where R_κ is the radius of the cavity mid-section normalized by the radius of the cone base, κ is the coefficient which value is close to 1 at the small cavitation numbers. In the first approximation we can neglect the dependence of κ on the Mach number. The solution for the thin cones has shown that at the constant value of L_k or L the value of R_κ remains the same at the variation of the Mach number. Then according to formula (1.1) the dependences $C_x(M)$ and $\sigma(M)$ must satisfy the following correlation

$$\frac{C_x(M)}{\sigma(M)} = const \qquad (1.2)$$

where the constant is the function of α and L_k. The calculations have shown that correlation (1.2) is satisfied with sufficient accuracy at the Mach numbers on the interval $0 \leq M \leq 0.8$ [13]. The cavity past a thin cone in incompressible fluid ($M=0$) has been considered as a particular case. The value of the cone apex half-angle equals $15°$. For this cone the results obtained based on the slender body theory have been compared with the results of the numerical calculation [15] for incompressible fluid. The comparison has shown good agreement of these results [13].

Let us consider the case when the parameter of the cavity thinness is far less than the parameter of the cavitator thinness. In this case we neglect the cavitator dimensions in comparison with the cavity dimensions. In order to determine the outer solution we assume that the radius of the cavitator equals zero. Let us place the origin of coordinates in the middle of the cavity length and the geometric dimensions normalize by the semi-length $L_k/2$. In this case integro-differential equation (2.6) in chapter 2 of lecture #1 takes the form [4,13]

$$\frac{u'^2}{2u} + u'' \ln \frac{(1-M^2)u}{4(1-x^2)} - \int_{-1}^{1} \frac{u''(x_1) - u''(x)}{|x-x_1|} dx_1 - \frac{u'(-1)}{1+x} + \frac{u'(1)}{1-x} = 2\sigma \qquad (1.3)$$

$$u = R^2, \quad R(\pm 1) = 0, \quad R(0) = \varepsilon_1$$

where $\varepsilon_1 = 2R_k / L_k = 1/\lambda$ is the small parameter equal to the inverse amount of the cavity aspect ratio λ.

We seek the outer solution in the form of expansion into asymptotic rows with the small parameter ε_1. For the squared cavity radius and the cavitation number these rows have the form

$$R^2 = \varepsilon_1^2 \left[R_0^2 + R_{-1}^2 \left(\ln \frac{1}{\varepsilon_1^2} \right)^{-1} + R_{-2}^2 \left(\ln \frac{1}{\varepsilon_1^2} \right)^{-2} + ... \right]$$

$$\sigma = \varepsilon_1^2 \left[\sigma_1 \left(\ln \frac{1}{\varepsilon_1^2} \right) + \sigma_0 + \sigma_{-1} \left(\ln \frac{1}{\varepsilon_1^2} \right)^{-1} + \dots \right] \tag{1.4}$$

After substitution of (1.4) in (1.3) and conservation of the two members of the rows integro-differential equation (1.3) is transformed to two differential equations. Solving the differential equations we obtain the expression for the cavity profile and the dependence of the cavitation number on the cavity aspect ratio and the Mach number [4,13]

$$R^2 = \varepsilon_1^2 \left\{ \left(1 - x^2\right) + \frac{x^2 \ln 4 - \ln\left[\left(1 + x\right)^{(1+x)}\left(1 - x\right)^{(1-x)}\right]}{2 \ln \lambda} \right\}$$

$$\sigma = \frac{2}{\lambda^2} \ln \frac{\lambda}{\sqrt{e}\sqrt{1 - M^2}} \tag{1.5}$$

where e is the base of natural logarithms.

The first approximation of the cavity profile is an ellipsoid of revolution (as in incompressible fluid). From the first expression (1.5) it follows that the added member to an ellipsoid is small at the small cavitation numbers, for example, then $\lambda=14.66$ and $\sigma=0.02$ ($M=0$) the difference between the cavity shape and an ellipsoid of revolution does not exceed 1%. In general the cavity aspect ratio is dependent upon the cavitation and Mach numbers. From the second expression (1.5) it follows that at the constant value of the cavity aspect ratio the cavitation number increases along with the Mach number. The analogous dependence is obtained in the case of the subsonic cavitation flow past a thin cone. As the cavitation number decreases the influence of fluid compressibility on the cavity aspect ratio becomes insignificant.

Thus, the investigation carried out on the basis of the slender body theory has shown that in subsonic flow we can neglect the influence of the Mach number on the cavity shape: the cavity shape is described by an ellipsoid of revolution with sufficient accuracy (as in incompressible fluid). An ellipsoid of revolution is obtained from the outer solution (1.5) (when we neglect the cavitator dimensions in comparison with the cavity dimensions) and from the solution for the thin cones ((2.9) in lecture #1) (when the parameter of the cavity thinness has the same order as the parameter of the cavitator thinness). The Mach number mainly influences the value of the cavitation drag of the cavitator (the cavitation drag coefficient increases along with the Mach number). At the constant cavity length the cavitation number increases along with the Mach number according to the law of conservation of momentum.

2. The application of the slender body theory for the investigation of supercavities in supersonic flow

Let us consider the cavitation flow past a thin cone in supersonic stream. We apply the Riabouchinsky scheme (Fig. 3 in lecture #1). The linearized equation for the perturbed velocity potential in the cylindrical coordinate system is written as following [16]

$$-\left(M^2 - 1\right)\frac{\partial^2 \varphi}{\partial x^2} + \frac{\partial^2 \varphi}{\partial r^2} + \frac{1}{r}\frac{\partial \varphi}{\partial r} = 0 \tag{2.1}$$

where $\varphi = \varphi * / V_0 R_n$ is the dimensionless perturbed velocity potential, $\varphi*$ is the perturbed velocity potential.

The geometric dimensions are scaled by the radius of the cone base (the description of the geometric dimensions is given in chapter 2 of lecture #1). For supersonic flow the perturbed velocity potential that satisfies equation (2.1) can be written in the form of integral [16]

$$\varphi = -\frac{1}{2\pi} \int_0^{x-\sqrt{M^2-1}r} \frac{q(x_1)dx_1}{\sqrt{(x-x_1)^2 - (M^2-1)r^2}} \qquad (2.2)$$

where $q(x_1)$ is the intensity of sources and sinks on the axis of symmetry. Near the surfaces of the thin cavitator and the cavity potential (2.2) that satisfies the kinematic boundary condition has the following asymptotic representation [17]

$$\varphi = \frac{1}{4\pi} S'(x) \ln \frac{(M^2-1)r^2}{4x^2} - \frac{1}{2\pi} \int_0^x \frac{S'(x_1) - S'(x)}{x-x_1} dx_1 \qquad (2.3)$$

where $S'(x)$ is the derivative of the dimensionless area of the cross section with respect to x coordinate.

For supersonic flow the dynamical boundary condition on the cavity surface has the same form as for subsonic flow [5] and is written as following

$$2\frac{\partial \varphi}{\partial x} + \left(\frac{\partial \varphi}{\partial r}\right)^2 = \sigma \qquad (2.4)$$

Substituting (2.3) in (2.4) we obtain the integro-differential equation for the cavity profile past a thin cone in supersonic flow

$$\frac{u'^2}{4u} + \frac{u''}{2} \ln \frac{(M^2-1)u}{4x^2} - \int_o^l \frac{u_1''(x_1) - u''(x)}{x-x_1} dx_1 - \int_l^x \frac{u''(x_1) - u''(x)}{x-x_1} dx_1 = \sigma \qquad (2.5)$$

$$u = R^2, \quad u_1 = R_1^2, \quad u_1'(0) = 0$$

We assume that the cone has the same thinness order as the cavity. The thinness order of the cone ε equals the ratio of the radius of the cone base to its height. We seek the solution for the whole area of the flow in the form of expansion into asymptotic rows with the small parameter ε. The rows have the form of correlations (1.4) if we substitute ε with ε_1. The boundary conditions are written in the same form as for subsonic flow [7,13]

$$x = l: \quad R = 1, \quad R' = \varepsilon$$

$$x = l + L_k : R = 1$$

After substitution of the asymptotic rows in (2.5) and conservation of the two members of rows integro-differential equation (2.5) is transformed to two differential equations. The first differential equation with the boundary conditions is written as follows

$$\frac{d^2 R_0^2}{dx^2} = -2\sigma_1$$

$$R_0^2(l) = l^2, \quad R_0^2(l + L_k) = l^2, \quad \frac{dR_0^2}{dx}\Big|_{x=l} = 2l \tag{2.6}$$

The solution of equation (2.6) has the form

$$R_0^2 = \sigma_1(a - x)(x - b)$$

$$\sigma_1 = \frac{2l}{L_k}, \quad a = \frac{L}{2} + \sqrt{\frac{L^2}{4} - \frac{lL}{2}}, \quad b = \frac{L}{2} - \sqrt{\frac{L^2}{4} - \frac{lL}{2}} \tag{2.7}$$

From expression (2.7) it follows that an ellipsoid of revolution is the first approximation of the cavity shape. The analogous result has been obtained in subsonic flow (expression (2.9) in lecture #1). The second approximation is determined from the differential equation which was obtained after equalization of members at ε^4.

In Fig. 4 the broken curve represents the first approximation of the cavity profile past the cone with the apex half-angle equal to 5°. The total length equals 200. The continuous curve represents the second approximation of the cavity profile.
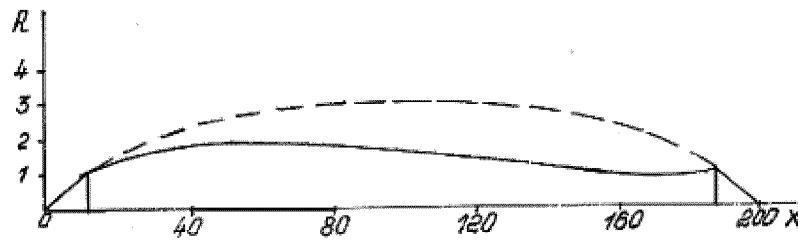

Fig. 4   Cavity profile in supersonic flow for the cone α=5°; the broken curve corresponds to the first approximation, the continuous curve corresponds to the second approximation

Figure 4 is analogous to Fig. 1 that illustrates the cavity profile past the same cone in subsonic flow. From Fig. 4 it follows that as distinct from subsonic flow (Fig. 1), in supersonic flow the second approximation of the cavity profile essentially differs from the first one, and the second members of asymptotic row are not smaller than the first ones. Besides, the unreal shape of the cavity contradicts with the physical laws of cavitation flows.

The analysis of this effect has shown that the slender body theory is not valid for the flow past the edge of the cone. In the supersonic flow the Prandtl-Meyer stream arises at the edge. The stream must turn at the angle that is dependent on the pressure within the cavity or the cavitation number. The

incline of a free stream line is less than the cone apex half-angle. It is impossible to satisfy this condition within the range of the slender body theory. The first peculiarity of the slender body theory application to the supersonic cavitation flow is its discrepancy with the boundary condition at the cavitator edge.

In order to determine the solution it is necessary to consider the supersonic flow around the cone, obtain the Mach number at its edge and match the Prandtl-Meyer stream with the cavitation flow. It is very difficult to carry out, as the cavity shape and the cavitation number are not known beforehand.

Let us determine the pressure coefficient on the surface of the thin cone in supersonic flow. The expression for the pressure coefficient has the form [16]

$$C_p = -2\frac{\partial \varphi}{\partial x} - \left(\frac{\partial \varphi}{\partial r}\right)^2 \tag{2.8}$$

where $C_p = 2(P_{con} - P_0)/\rho V_0^2$ is the pressure coefficient, P_{con} is the pressure on the cone surface.

After differentiating expression (2.3) the components of the perturbed velocity on the cone surface are written as following

$$\frac{\partial \varphi}{\partial x} = \frac{\varepsilon^2}{2}\ln\frac{(M^2-1)\varepsilon^2}{4}$$
$$\frac{\partial \varphi}{\partial r} = \varepsilon \tag{2.9}$$

After substitution of (2.9) in (2.8) for the pressure coefficient we obtain the following expression

$$C_p = -\varepsilon^2\left[\ln\frac{(M^2-1)\varepsilon^2}{4} + 1\right] \tag{2.10}$$

Formula (2.10) coincides with the expression that defines the pressure coefficient on the thin cone in supersonic flow of air [16]. The pressure coefficient is connected to the cavitation drag coefficient by the following dependence

$$C_x = 2\varepsilon\int_0^l C_p R_1(x)dx + \sigma \tag{2.11}$$

where C_x is the cavitation drag coefficient normalized by the area of the cone base; $R_1(x) = \varepsilon x$ is the radius of the cone cross section.

The pressure coefficient is constant on the cone surface and expression (2.11) takes the form

$$C_x = C_p + \sigma \tag{2.12}$$

We can consider the coefficient C_p to be the cavitation drag coefficient at the zero cavitation number C_{xo}. The formula is written as follows

$$C_x = C_{xo} + \sigma \qquad (2.13)$$

Expression (2.13) is the dependence of the cavitation drag coefficient on the cavitation number at the constant Mach number.

Let us consider the case when the parameter of the cavity thinness is far less than the parameter of the cavitator thinness. A similar case was considered for subsonic flow in chapter 1. Let us place the origin of coordinates in the middle of the cavity length and normalize the geometric dimensions by the semi-length $L_k/2$. Integro-differential equation (2.5) takes the form

$$\frac{u'^2}{4u} + \frac{u''}{2}\ln\frac{(M^2-1)u}{4(x+1)^2} - \int_{-1}^{x}\frac{u''(x_1)-u''(x)}{x-x_1}dx_1 - \frac{u'(-1)}{x+1} = \sigma$$

$$u = R^2, \quad R(\pm 1) = 0, \quad R(0) = \varepsilon_1 \qquad (2.14)$$

where $\varepsilon_1 = 2R_k/L_k = 1/\lambda$ is the small parameter equal to the inverse amount of the cavity aspect ratio λ.

For determination of the outer solution we neglect the cavitator dimensions in comparison with the cavity dimensions (the radius of the caivtator equals zero in (2.14)). We seek the outer solution in the form of expansion into asymptotic rows with the small parameter ε_1. For the cavity radius squared and the cavitation number these rows have the form (1.4). After substitution of (1.4) in (2.14) and conservation of the two members of the rows integro-differential equation (2.14) is transformed to two differential equations. Solving the differential equations we obtain the expression for the cavity profile and the cavitation number dependence on the cavity aspect ratio and the Mach number

$$R^2 = \varepsilon_1^2\left\{(1-x^2) + \frac{x^2\ln 4 + \ln\left[(1+x)^{(x^2-x-2)}(1-x)^{(x-x^2)}\right]}{2\ln\lambda}\right\}$$

$$\sigma = \frac{2}{\lambda^2}\ln\frac{\lambda}{\sqrt{e}\sqrt{M^2-1}} \qquad (2.15)$$

The comparison of the dependences (2.15) with the analogous ones (1.5) obtained for subsonic flow shows that in supersonic flow the first approximation of the cavity shape is an ellipsoid of revolution (as in incompressible fluid). The numerator of the second member in the asymptotic row (2.15) can be presented as the sum of two functions $f_1(x)$ and $f_2(x)$

$$f_1(x) = x^2\ln 4 - \ln\left[(1+x)^{(1+x)}(1-x)^{(1-x)}\right]$$

$$f_2(x) = \ln\left[(1+x)^{(x^2-1)}(1-x)^{(1-x^2)}\right]$$

The function $f_1(x)$ corresponds to the second approximation of the cavity profile in subsonic flow (1.5). In case of supersonic flow the odd function $f_2(x)$ is added to the even function $f_1(x)$ and the cavity becomes asymmetric relatively to the middle of its length. The cavity asymmetry is explained by the fact

that in supersonic flow the influence of sources and sinks spreads downstream only. The expression for $f_2(x)$ shows that $f_2(x)>0$ at $x<0$ and $f_2(x)<0$ at $x>0$, i.e. the cavity is thicker in the head than in the back part and the mid-section displaces ahead.

The calculations have shown that at the cavitation numbers that have the order 10^{-2} the second approximation of the cavity shape in (2.15) is close to the first one and the difference does not exceed several percent. From the second expression (2.15) it follows that the cavity aspect ratio is dependent upon the cavitation and Mach numbers. As the cavitation number decreases the influence of the fluid compressibility on the cavity aspect ratio becomes insignificant.

3. The application of the numerical methods for calculation of supercavities in subsonic flow

The modern numerical methods enable us to calculate the cavitation flows in compressible fluid efficiently. The author has worked out the algorithm of calculation of axisymmetric cavities in sub- and supersonic compressible fluid flow over a wide range of cavitation numbers [11,12].

Let us consider axisymmetric subsonic cavitation flow past a disk in accordance with the Riabouchinsky scheme; in this scheme the cavity is closed by a disk of the same dimensions as the cavitator disk (Fig. 5)
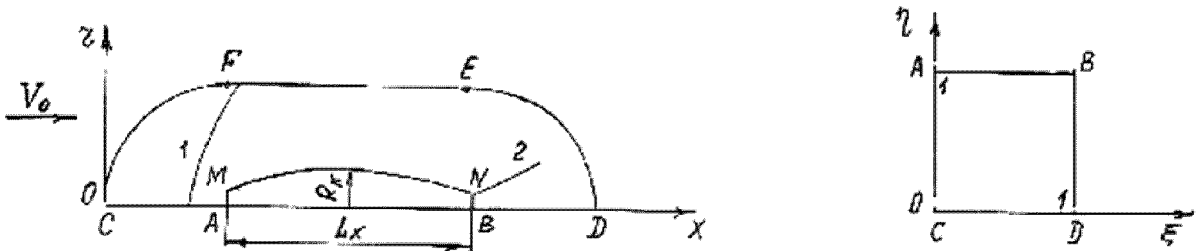

Fig. 5   Flow schematic and computation domain. 1 is the forward shock, 2 is the trailing shock

In view of the flow symmetry, we will examine the flow in a meridional plane. The problem consist in determining the shape of the cavity boundary MN that satisfy the constant velocity and impermeability conditions for a given cavity length L_k (see Fig. 5 where AM is the disk-cavitator, NB is the closing disk, CFED is the external boundary). The geometric dimensions are scaled by the disk radius. The external boundary CFED consists of three parts: CF and ED are parts of the circles with radius 120 and centers at the points A and B respectively; the segment FE is a parallel to the axis of symmetry and located at a distance of 120 from the latter. As the main equation we use the equation of continuity

$$\frac{\partial}{\partial x}\left(\rho v_x r\right)+\frac{\partial}{\partial r}\left(\rho v_r r\right)=0 \tag{3.1}$$

where v_x and v_r are the velocity components in the x and r directions respectively. The flow velocity and liquid density are scaled by the free stream velocity V_0 and density ρ_0 respectively. In the

compressible case equation (3.1) is essentially nonlinear, and we will apply the finite-difference method to solve it. The density-velocity relationship is taken from the Bernoulli equation

$$\rho = \left[1 + \frac{(n-1)M^2}{2}\left(1 - v_x^2 - v_r^2\right)\right]^{1/(n-1)}, n = 7.15 \tag{3.2}$$

In order to make the formulation of the boundary conditions at the cavity surface more convenient, it makes sense to map the computational domain in x, r coordinates onto a unit square in ξ, η coordinates, conformity of the points is shown in Fig. 5. After mapping equation (3.1) takes the form [18]

$$\frac{\partial}{\partial \xi}\left(\frac{\rho r U^c}{J}\right) + \frac{\partial}{\partial \eta}\left(\frac{\rho r V^c}{J}\right) = 0$$

$$U^c = \frac{\partial \xi}{\partial x}v_x + \frac{\partial \xi}{\partial r}v_r, \quad V^c = \frac{\partial \eta}{\partial x}v_x + \frac{\partial \eta}{\partial r}v_r \tag{3.3}$$

$$J = \frac{\partial \xi}{\partial x}\frac{\partial \eta}{\partial r} - \frac{\partial \xi}{\partial r}\frac{\partial \eta}{\partial x}$$

where U^c and V^c are the contravariant velocity components in the ξ and η directions, and J is the Jacobian of the mapping. We consider the flow to be potential and write the velocity components in the following form [18]

$$U^c = A_1 \frac{\partial \Phi}{\partial \xi} + A_3 \frac{\partial \Phi}{\partial \eta}, \quad V^c = A_3 \frac{\partial \Phi}{\partial \xi} + A_2 \frac{\partial \Phi}{\partial \eta}$$

$$A_1 = \left(\frac{\partial \xi}{\partial x}\right)^2 + \left(\frac{\partial \xi}{\partial r}\right)^2, \quad A_2 = \left(\frac{\partial \eta}{\partial x}\right)^2 + \left(\frac{\partial \eta}{\partial r}\right)^2$$

$$A_3 = \frac{\partial \xi}{\partial x}\frac{\partial \eta}{\partial x} + \frac{\partial \xi}{\partial r}\frac{\partial \eta}{\partial r}$$

where Φ is the flow velocity potential and A_1, A_2, A_3 are metric coefficients. After mapping onto ξ, η plane equation (3.2) takes the form

$$\rho = \left[1 + \frac{(n-1)M^2}{2}\left(1 - \frac{\partial \Phi}{\partial \xi}U^c - \frac{\partial \Phi}{\partial \eta}V^c\right)\right]^{1/(n-1)} \tag{3.4}$$

The boundary condition is the following: the tangential velocity is constant on the cavity boundary MN, the impermeability condition is imposed on the segments CA, AM, NB and BD, the potential on the external boundary is equal to the free stream potential.

Thus, in order to determine the cavitation flow it is necessary to solve equation (3.3) onto a unit square with the given boundary conditions. The dependence of the density on the velocity (3.4) is added to equation (3.3). The entire computational domain (that is the unit square in the ξ, η plane) is divided by a network with steps $\Delta\xi$ and $\Delta\eta$ along ξ, and η directions.

The non-linear system of equations obtained as a result of the discretization was solved using the iteration method with approximate factorization [18]. Before proceeding to the calculations the first approximation for the cavity shape between the points M and N was preassigned and the computational network corresponding with the given cavity was constructed using an algebraic mapping technique [18]. The velocity on the cavity surface V_k was determined on each iteration stage using the values of the potentials Φ_N, Φ_M at the points N and M from the correlation

$$V_k = \left(\Phi_N - \Phi_M\right)/s_N$$

s_N is the length of the arc measured from the disk edge M to the point N on the closing disk. The potential at the point on the cavity surface corresponding to s is given by the expression

$$\Phi(s) = V_k s + \Phi_M \qquad (3.5)$$

where s is the arc length measured from the point M to the given point on the cavity surface. This expression was used for specifying the boundary conditions on the segment MN.

The iteration procedure turned out to be convergent; the discrepancy diminished, and the potential increment vanished as the number of the iteration cycles increased. However, in general, the obtained solution did not satisfy the impermeability condition on the cavity surface. In order to satisfy the impermeability condition the cavity shape was varied using the following way [11]. The normal flow velocity on the cavity surface was represented in the form - $\partial\Phi/\partial n = \partial\varphi/\partial n + \partial x/\partial n$ where φ is the perturbed velocity potential, x is the coordinate of a point on the cavity surface, n is the normal to the surface, and $\partial x/\partial n = \partial r/\partial s$. The cavity shape must satisfy the impermeability condition $\partial\Phi/\partial n = 0$ or

$$\frac{\partial r}{\partial s} = -\frac{\partial\varphi}{\partial n} \qquad (3.6)$$

In [11] it is shown that for subsonic flow in view of cavity symmetry about the mid-section the iteration process of solving the system of two first order differential equations converges precisely to relation (3.6). The system has the form

$$\frac{\partial r}{\partial s} = -\frac{\partial\varphi}{\partial n}, \quad \frac{\partial x}{\partial s} = \sqrt{1 - \left(\frac{\partial r}{\partial s}\right)^2} \qquad (3.7)$$

According to equations (3.7) the front half of the cavity had to be corrected.

The numerical analysis was performed for the constant cavity length $L_k=199.96$ that corresponds with the cavitation number 0.02 for incompressible fluid. The results of the numerical calculations were checked on the satisfaction of the mass and momentum conservation laws and were compared with the results obtained by the slender body theory. The numerical calculations show that in subsonic flow the

cavity shape is close to an ellipsoid of revolution and the dependence $\sigma(\lambda, M)$ is described by the the second expression (1.5) with sufficient accuracy. Moreover, the test calculations were performed to compare with results [15] for incompressible fluid ($M=0$, $\sigma=0.02$) and results [10] ($M=0.5$ $\sigma=0.16$). The comparison has shown a good agreement. For subsonic flow the cavity shape in the vicinity of the disk is shown in Fig. 4 in lecture #1. The continuous curve represents the calculations [15] for incompressible fluid. The author's numerical results are shown by points for different Mach numbers. In Fig. 5 in lecture #1 we compare the cavity profiles in compressible and incompressible fluid for the same cavitation number $\sigma=0.0235$. The continuous curve corresponds to the cavity profile in compressible fluid calculated by the numerical method for $M=0.8$; the broken curve corresponds to the cavity in incompressible fluid calculated by Logvinovich formula [14].

4. The application of the numerical methods for calculation of supercavities in supersonic flow

Let us consider axisymmetric supersonic cavitation flow past a disk in accordance with the Riabouchinsky scheme. The proposed flow scheme is presented in Fig. 5. In case of supersonic flow the shock waves appear (see Fig. 5, curve 1 is the forward shock formed upstream of the disk, and curve 2 is the trailing shock emanating from the closing disk edge). The forward shock is the most intense and nearly normal in the vicinity of the symmetry axis.

However, the shocks appearance does not break the condition that the flow is potential. In water over a wide range of pressures a shock adiabat agrees with the static one expressed by the Tait equation [19]. The special investigation on the analysis of the shock equations was carried out [20]. The analysis has shown that we can assume that the normal shock in water is isentropic and the flow is potential if Mach number does not exceed the value 2.2. In [20] it is shown that we can determine the density from the Bernoulli equation (3.2) in the whole area of the supersonic flow (at the known flow velocity).

Thus, the main equations for the calculation of the supersonic cavitation flow are equations (3.3) and (3.4) as in case of subsonic flow. We will apply the finite-difference method to solve these equations [12]. As distinct from the subsonic flow, in the supersonic flow the boundary conditions on the external boundary are the following: the potential is equal to the free stream potential only on the part of the external boundary where the normal velocity directed along the external normal is less than the velocity of sound. On the part of the external boundary where the normal velocity is more than the velocity of sound the potential is determined by interpolation of values in the nearest nodes of the computational network. As distinct from the subsonic flow, we apply the artificial viscosity so that the difference scheme will be stable in the supersonic area [18,21]. The artificial viscosity is introduced as a modification of density expression [12]. The modification is equivalent to upstream displacement of the computation domain nodes.

The non-linear system of equations obtained as a result of the discretization was solved using the iteration method with approximate factorization [12] (as in case of subsonic flow). The iteration procedure turned out to be convergent; the discrepancy diminished, and the potential increment vanished as the number of the iteration cycles increased. However, in general, the obtained solution did not satisfy the impermeability condition on the cavity surface. In case of subsonic flow the impermeability condition was satisfied by varying the cavity shape with the help of equations (3.7) which are first order differential equations, and since at subsonic flow velocities the cavity is symmetric with respect to the mid-section, a single boundary condition sufficed and only the front half of the cavity had to be corrected. However, at supersonic flow velocities the cavity is asymmetric and its shape must be corrected using second order differential equations subject to the boundary conditions

$$s = 0: \quad r = 1, \quad x = 0$$

$$s = s_N: \quad r = 1, \quad x = L_k$$

The cavity shape was corrected from the disk-cavitator edge towards the closing disk edge. The system of differential equations was derived by differentiating (3.7) with respect to s

$$\frac{\partial^2 r}{\partial s^2} = -\frac{\partial}{\partial s}\left(\frac{\partial \varphi}{\partial n}\right), \quad \frac{\partial^2 x}{\partial s^2} = -\frac{\partial r}{\partial s}\frac{\partial^2 r}{\partial s^2}\left[1 - \left(\frac{\partial r}{\partial s}\right)^2\right]^{-1/2} \tag{4.1}$$

Note that the second derivative d^2r/dx^2 has a singularity near the disk edge, an accurate determination of the second derivatives in (4.1) presents considerable difficulties in this area. The calculation of the second derivatives near the disk edge was avoided by using equations (4.1) for $2 < x < L_k - 2$, and in the vicinity of the cavitator and closing disk the cavity shape was corrected using equations (3.7) (as in subsonic flow). As a result of the numerical solution the obtained cavity shape satisfied both the constant velocity condition (3.5) and the impermeability condition (3.6).

The numerical analysis was performed for the constant cavity length $L_k=199.96$ that corresponds with the cavitation number 0.02 for incompressible fluid. Calculations of supercavities downstream of a disk within the range of Mach numbers $1 \leq M \leq 1.4$ have been performed. As a result of the analysis for different Mach numbers the following characteristics were defined – the cavitation number, the cavitation drag ratio, the mid-section radius, the aspect ratio, the cavity shape, and the shock's distance from a disk.

The results of the numerical calculations of the supercavities in supersonic flow satisfy the mass and momentum conservation laws. For the supersonic flow the cavity shape defined by the numerical calculation is close to an ellipsoid of revolution. It agrees with the author's results obtained with the help of the slender body theory (see chapter 2). However, the results on asymmetry of the cavity shape (mid-section displacement relative to the middle of the cavity length) do not agree. While the numerical calculation yields a displacement directed downstream, in chapter 2 (the first expression (2.15)) an opposite displacement was obtained. The behavior of the dependence of σ on λ and M is also different: for constant L_k the calculated aspect ratio and σ increase with the increase in the Mach number (as in subsonic flow), whereas the second expression (2.15) yields the opposite. The discrepancy is due to the fact that the search for the second approximation to the cavity shape and the dependence $\sigma(\lambda, M)$ carried out in chapter 2 overstepped the limits of the slender body theory for supersonic flow. In fact, the first approximation (an ellipsoid of revolution) is not a slender body in the front part where the shock arises. The shock is not described by the small perturbation theory. This is the second peculiarity of the slender body theory application to the supersonic cavitation flows that should be noted.

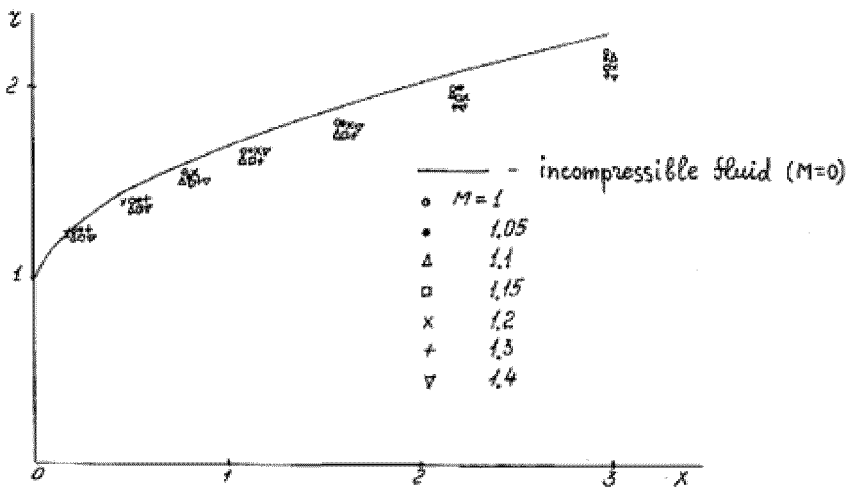The cavity profile in the vicinity of the disk is shown in Fig. 6.

Fig. 6   The front of the cavity

The continuous curve represents the calculation for incompressible fluid [15]. The author's numerical results for supersonic flow are shown by points for different Mach numbers. It can be seen that in supersonic flow the cavity in initial regions is narrower than in incompressible flow. Narrowing of the cavity is related to the Prandtl-Meyer stream at the disk edge.
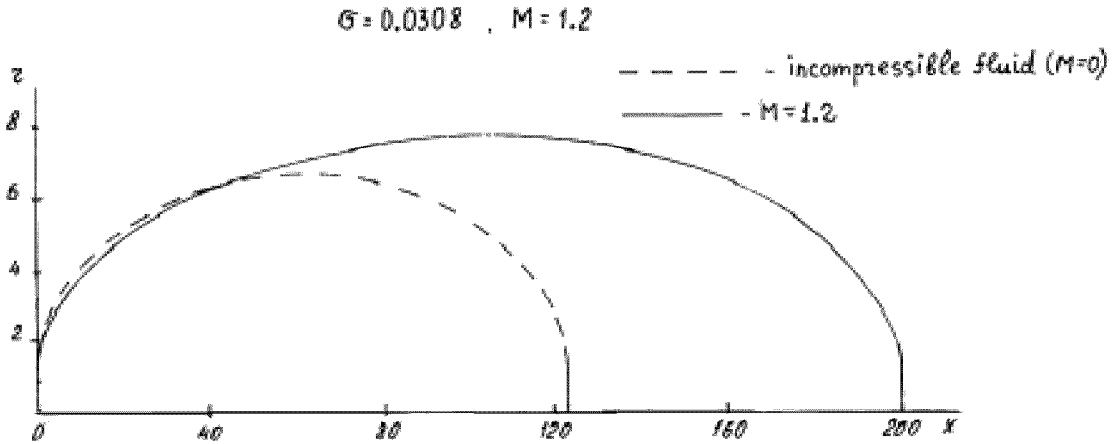

Fig. 7   Cavity profile

In Fig. 7 we compare the cavity profile in supersonic flow and incompressible fluid for the same cavitation number $\sigma=0.0308$. The continuous curve corresponds to the numerical method for $M=1.2$, the broken curve corresponds to the cavity in incompressible fluid. The maximum asymmetry to the cavity shape was observed for the Mach number equal to 1.1 (this case is illustrated in Fig. 8)
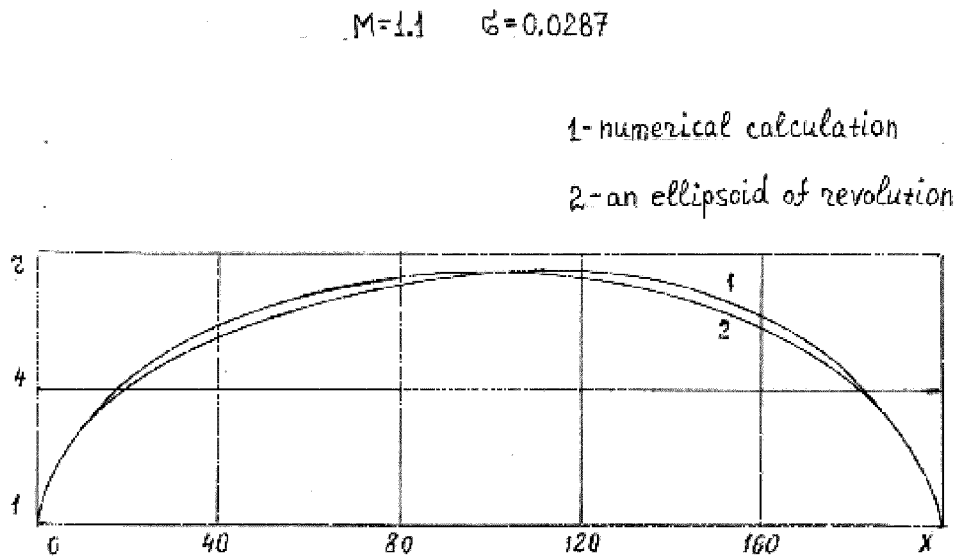

Fig. 8   Cavity profile

In Fig. 8 curve 1 corresponds to the numerical calculation, curve 2 corresponds to an ellipsoid of revolution (the origin is on the disk edge). From Fig. 8 it is evident that in the first approximation the cavity profile is close to an ellipsoid of revolution in supersonic flow.

The positions of the forward shock and the sonic line (where the local Mach number equals 1) were determined by numerical calculation. It was found that in case of supersonic cavitation flow past a disk the distance between the forward shock and the disk surface is much greater that in case of continuous supersonic air flow [12].
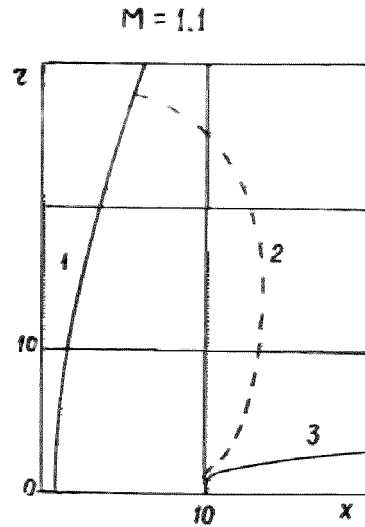

Fig. 9   Position of the forward shock for *M*=1.1. 1 is the forward shock, 2 is the sonic line and 3 is the cavity front profile.

As an example, in Fig. 9 the position of the forward shock is shown for the Mach number equal to 1.1. Curve 1 corresponds to the forward shock; curve 2 corresponds to the sonic line: curve 3 corresponds to the cavity front profile. The Mach number dependence of the cavitation drag coefficient of a disk at zero cavitation number C_{xo} is shown in Fig. 10 [12].
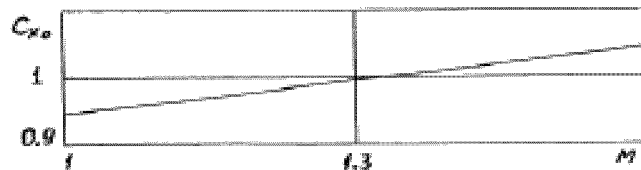

Fig. 10   Dependence of C_{xo} on M

Based on the numerical calculations we can conclude that the passing through the speed of sound does not result in a substantial variation in the cavity shape as compared with subsonic flow. In agreement with the slender body theory, the cavity shape in supersonic flow is close to an ellipsoid of revolution.

5. Shocks in a supersonic water stream

We will consider an oblique shock in a supersonic water flow, the double line in Fig. 11, where β is the angle between the direction of the undisturbed velocity V_0 and the shock, θ is the angle of deviation of the flow behind the shock, v_{no} and $v_{\tau o}$ are the normal and tangential components of the velocity ahead of the shock, and v_{n1} and $v_{\tau 1}$ are the velocity components behind the shock.
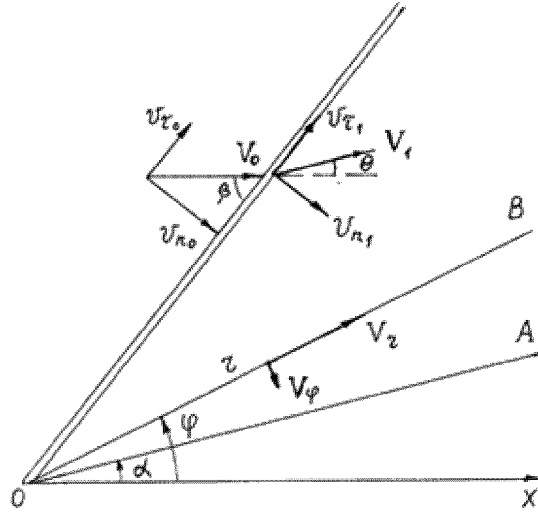

Fig. 11   Oblique shock and diagram of supersonic flow past a cone OA

The basic relations for the shock, namely, the mass and momentum conservation equations can be written as follows [22]

$$\rho_0 v_{no} = \rho_1 v_{n1} \tag{5.1}$$

$$\rho_0 v_{no}^2 + P_0 = \rho_1 v_{n1}^2 + P_1 \tag{5.2}$$

$$v_{\tau_0} = v_{\tau 1} \tag{5.3}$$

where P_0, ρ_0 are the pressure and the density ahead of the shock, and subscript 1 denotes the quantities behind the shock.

The equation of the shock adiabatic curve must be added to equations (5.1)-(5.3). It is well known [19] that at the pressures lower than $3 \cdot 10^3$ MPa the shock and the static adiabatic curves coincide and can be expressed by the Tait equation

$$P_1 - P_0 = B\left[\left(\frac{\rho_1}{\rho_0}\right)^n - 1\right], \quad B = \frac{\rho_0 a_0^2}{n}, \quad n = 7.15 \tag{5.4}$$

where a_0 is the speed of sound in the free stream ahead of the shock.

If on the shock front the pressure exceeds the value $3 \cdot 10^3$ MPa, the equation of the shock adiabatic curve can be written in the form [19]

$$P_1 - P_0 = d\left[\left(\frac{\rho_1}{\rho_0}\right)^k - 1\right], \quad d = 416 MPa, \quad k = 6.29 \tag{5.5}$$

Behind the shock the speed of sound $\left(a_1^2 = dP / d\rho\right)$ can be determined from the static adiabat (5.4)

$$a_1^2 = a_0^2 \left(\frac{\rho_1}{\rho_0}\right)^{n-1} \tag{5.6}$$

The expressions for determining the flow velocities ahead of the shock V_0 and behind it V_1 have the form

$$V_0 = \sqrt{v_{no}^2 + v_{\tau 0}^2}, \quad V_1 = \sqrt{v_{n1}^2 + v_{\tau 1}^2}$$

The dependences of the ratio of densities ρ_0/ρ_1 on the free stream Mach number ($M = V_0/a_0$) come from equations (5.1)-(5.3), (5.4) and (5.5) and can be written as follows

$$M^2 \sin^2 \beta = \left[\left(\frac{\rho_1}{\rho_0}\right)^n - 1\right]\left[n\left(1 - \frac{\rho_0}{\rho_1}\right)\right]^{-1}$$

$$M^2 \sin^2 \beta = \left[\left(\frac{\rho_1}{\rho_0}\right)^k - 1\right]\frac{d}{\rho_0 a_0^2}\left(1 - \frac{\rho_0}{\rho_1}\right)^{-1} \tag{5.7}$$

We apply the first expression (5.7) when on the shock front the pressure does not exceed the value $3 \cdot 10^3$ MPa ($M\sin\beta \leq 2.2$), the second expression (5.7) corresponds to the pressure that exceeds this value.

Let us consider a particular case that corresponds to the normal shock ($\beta = 90°$). For this case the following correlations are satisfied

$$v_{\tau 0} = v_{\tau 1} = 0, \quad V_0 = v_{no}, \quad V_1 = v_{n1}, \quad \sin \beta = 1$$

The quantity of perturbed velocity u behind the shock is determined from the expression

$$u = V_0 - V_1 \tag{5.8}$$

The following is the way how we can calculate the flow parameters behind the normal shock. The value of the pressure on the shock front P_1 is given, then from (5.4) or (5.5) the ratio of densities ρ_1/ρ_0 is calculated. From expressions (5.7) the Mach number and velocity V_0 are determined, from (5.1) the value of velocity behind the shock V_1 is found. Then from equations (5.6) and (5.8) the speed of sound behind the shock a_1 and perturbed velocity u are determined. With the help of formulas (5.1), (5.2), (5.4)-(5.8) the author has calculated the flow parameters behind the normal shock on the pressure P_1 interval 490MPa$\leq P_1 \leq$7840 MPa [20]. The results of this calculation have been compared with the results [23] obtained from the mass, momentum and energy conservation equations which were solved by the method of successive approximations. The flow parameters calculated by the author (V_0, u, a_1), and determined in [23] at the same values P_1 (V_0', u', a_1') are presented in the table.

TABLE

P_1, MPa	V_0, m/s	V_0', m/s	u, m/s	u', m/s	a_1, m/s	a_1', m/s
490	1967	1975	249	251	2221	2230
980	2310	2335	424	426	2734	2755
1470	2586	2630	568	567	3142	3175
1960	2823	2880	694	689	3491	3535
2450	3033	3110	808	798	3798	3855
2940	3223	3320	912	898	4075	4140
3430	3394	3510	1011	990	4343	4405
3920	3550	3690	1104	1075	4605	4650
4900	3836	4020	1277	1235	5088	5100
5880	4095	4325	1436	1380	5527	5505
6860	4333	4610	1583	1510	5931	5880
7840	4554	4885	1722	1625	6309	6240

From the table it is evident that the results obtained by the author is close to the results obtained in [23]. Consequently we can use expressions (5.4) and (5.5) for calculation of the shock adiabatic curve. It should be noted that T. Nishiyama in [9] applied the equations identical to the relations for a normal shock in air for calculation of a normal shock in water. In [24] it is shown that the equations in [9] are not applicable for calculating the shocks in water and they contradict with the well-known experimental and theoretical results.

Let us continue the consideration of the oblique shock. Expressions for the flow turning angle θ and the Mach number $M_1 = V_1 / a_1$ behind the shock can be determined from equations (5.1)-(5.3) and (5.6) and the geometric relations in Fig. 11.

$$\frac{tg(\beta - \theta)}{tg\beta} = \frac{\rho_0}{\rho_1}, \quad M_1 = \frac{M\sin\beta}{\sin(\beta - \theta)}\left(\frac{\rho_0}{\rho_1}\right)^{(n+1)/2} \tag{5.9}$$

The flow turning angle θ was calculated at Mach numbers on the interval $1.2 \leq M \leq 5$ [25]. The calculation was performed as follows. For the chosen value of M the interval of shock angle β (from Mach angle equal to arcsin $1/M$ to $\pi/2$) was divided into 200 parts; for the chosen values of M and β the ratio of densities ρ_0/ρ_1 was determined from (5.7) by half-division method. The value of ρ_0/ρ_1 was substituted in the first equation (5.9) and the value of θ was determined. The Mach number M_1 was determined from the second equation (5.9). In Fig. 12 we have reproduced the calculation results in the form of graphs of θ versus β at various M (continuous curves 1-8, the Mach numbers equal 1.2; 1.4; 1.6; 2; 2.5; 3; 4; 5 respectively).
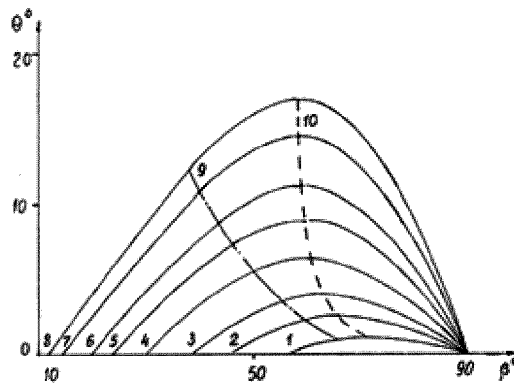

Fig.12 **Dependence of θ on β; curves 1-8 correspond to-M=1.2; 1.4; 1.6; 2; 2.5; 3; 4 and 5; curve 9 and 10 correspond to M_1=1 and-θ =θ* respectively**

The chain curve 9 separates the domains of supersonic flow behind the shock (M_1>1) and subsonic flow, the domains of supersonic flow are located to the left curve 9. The broken curve 10 corresponds to the maximum (critical) angles θ*. The domain to the right of curve 10 corresponds to a detached shock. If the apex angle of the wedge exceeds the value of 2θ* then the flow around this body has the curved detached shock. In Fig. 13 curve 1 represents the graph of the critical angle θ* as a function of M for a wedge.
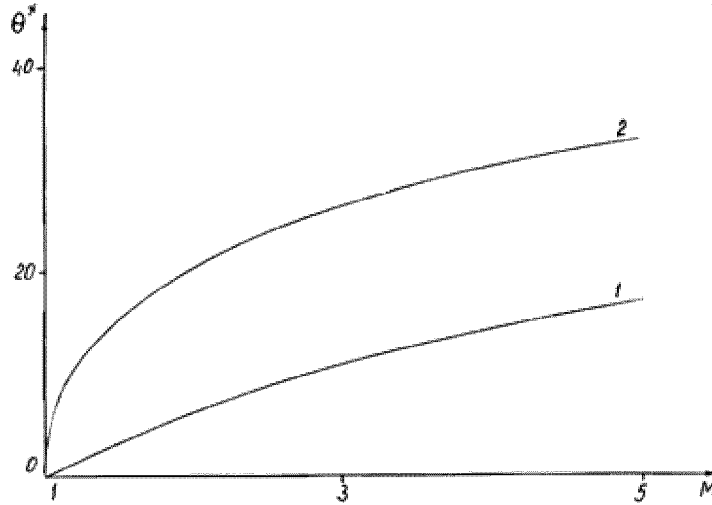
Fig.13 Dependence of θ^* on M; curves 1 and 2 correspond to flow past a wedge and cone respectively

6. Conical flows

Let us consider the axisymmetric conical flow formed behind a shock (Fig. 11) [25]; the line OA is the profile of the cone and α is its apex half-angle. The spherical coordinate system φ, r with the origin that lies at the apex of the cone and with x-axis directed along the symmetry axis is introduced. The angle φ is measured from the x-axis, r-coordinate equals the radius-vector drawn from the origin, OB is the intermediate conical surface, V_r is the component of the velocity directed along the radius-vector, V_φ is the component of the velocity directed along the perpendicular to the radius-vector.

The basic condition of the conical flow concludes that the flow parameters must be constant along the straight lines drawn from the apex of the cone. Consequently, any partial derivative of the flow parameters with respect to r – coordinate equals zero. The equations that define the kinematic parameters of the conical flow have been obtained from the continuity and Euler equations [22]

$$\frac{dV_\varphi}{d\varphi} = \frac{2a^2 V_r + a^2 V_\varphi ctg\varphi - V_r V_\varphi^2}{V_\varphi^2 - a^2}, \quad \frac{dV_r}{d\varphi} = V_\varphi \tag{6.1}$$

where a is the speed of sound at the given point of the flow.

For the velocity components $V_{\varphi 1}$ and V_{r1} the boundary conditions on the shock are written as follows

$$V_{\varphi 1} = -V_0 \sin\beta \frac{\rho_0}{\rho_1}, \quad V_{r1} = V_0 \cos\beta, \quad \varphi = \beta \tag{6.2}$$

The boundary conditions on the cone surface have the form

$$V_\varphi = 0, \quad V_r = V_{con}, \quad \varphi = \alpha \tag{6.3}$$

where V_{con} is the quantity of the velocity on the cone surface.

The speed of sound in the region behind the shock is determined from the Bernoulli equation

$$\frac{1}{2}\left(V_{\varphi 1}^2 + V_{r1}^2\right) + \frac{a_1^2}{n-1} = \frac{1}{2}\left(V_{\varphi}^2 + V_r^2\right) + \frac{a^2}{n-1} \tag{6.4}$$

The dependence of the density on the speed of sound has the form

$$\rho = \rho_1 \left(\frac{a}{a_1}\right)^{2/(n-1)} \tag{6.5}$$

The pressure in regions behind the shock is calculated from the static adiabatic curve at the known value of the density

$$P - P_1 = \frac{\rho_1 a_1^2}{n}\left[\left(\frac{\rho}{\rho_1}\right)^n - 1\right] \tag{6.6}$$

The conical flow behind the shock has been calculated in the following way. The system of equations (6.1), the boundary conditions (6.2) and (6.3) and equation (6.4) were reduced to the dimensionless form. The quantity of the velocity was normalized by the free stream speed of sound a_0 and we obtained the Mach number M as the dimensionless parameter. The Mach number was specified on the interval $1 < M \leq 5$. For the chosen M the interval of shock angle β (from Mach number to $\pi/2$) was divided into 200 parts. Then for the chosen values of M and β from (5.7) and (6.1)-(6.4) the apex half-angle of the cone α was calculated. The system of differential equations (6.1) was solved by the numerical Runge-Kutta method. As the boundary condition we applied condition (6.2) and the step of angle change $\Delta\varphi$ was equal to $0.25°$. The condition (6.3) was used to determine the end of counting. The segment $[\varphi_i, \varphi_{i+1}]$ was determined on which the value of V_φ reversed sign. Then on this segment the value of α that corresponds to the condition $V_\varphi = 0$ was found. As a result of these calculations for the fixed values of M we have obtained the dependences $\alpha(\beta)$, $M_{con}(\beta)$, $V_{con}(\beta)$ ($M_{con} = V_{con}/a_{con}$, where a_{con} is the speed of sound on the cone surface).

From the dependences $\alpha(\beta)$ the maximum angles α corresponding to the critical cone angles θ^* were determined for all values of M. If the cone apex half-angle α exceeds the value of θ^* then the supersonic flow around this body has the curved detached shock and the conical flow behind the shock is absent. In Fig. 13 curve 2 represents the graph of θ^* as a function of M. A comparison of the results in Fig. 13 with the results for air [22] shows that in supersonic water flow past a wedge or cone the critical angles are significantly less than those in an air flow past the same bodies.

For the visual representation the found values of β, α, V_{con} and M_{con} were treated and the dependences $\beta(M)$, $V_{con}(M)$ and $M_{con}(M)$ were obtained for the fixed values of α. The treatment was performed by interpolation. The values of cone angles α were chosen equal to $5°$, $10°$, $15°$, $20°$, $25°$ and $30°$. Using the value of the velocity on the cone surface V_{con} the pressure coefficient C_p was calculated from equations (6.4), (6.5) and (6.6).

In Fig. 14 we have plotted graphs of the angle β of inclination of the shock as a function of M at cone angles $5° \leq \alpha \leq 30°$ (curves 1-6).
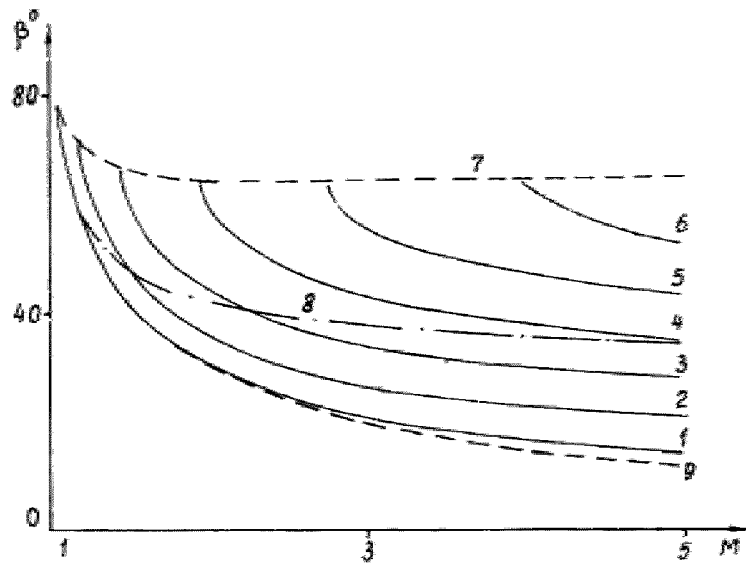
Fig. 14 Dependence of β on M; curves 1-6 correspond to α=5°, 10°, 15°, 20°, 25° and 30°; curve 7 corresponds to detachment of the shock from the apex of the cone; curve 8 corresponds to M_{con}=1; curve 9 corresponds to the Mach line ($sin\beta$=1/M)

The broken curve 7 corresponds to detachment of the bow shock from the apex of the cone. The chain curve 8 separates the domains of supersonic (M_{con}>1) and subsonic flows on the cone, the supersonic domain is located below curve 8. The broken curve 9 corresponds to the Mach angle ($sin\beta$=1/M). From Fig. 14 it is evident that the bow shock for the cone α=5° is Mach shock, it is close to the Mach line. We can assume that the flow around this cone is described by the small perturbation theory.
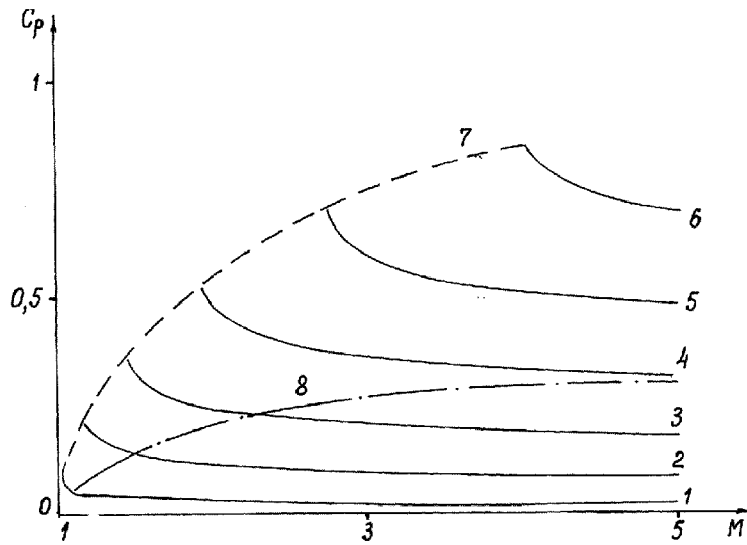

Fig. 15 Dependence of C_p on M; curves 1-6 correspond to α=5°, 10°, 15°, 20°, 25° and 30°; curve 7 corresponds to the detachment of the shock from the apex of the cone; curve 8 corresponds to M_{con}=1

In Fig.15 we have plotted graphs of the pressure coefficient C_p as a function of M for various cone angles (curves 1-6). The broken curve 7 and the chain curve 8 have the same meaning as those in Fig. 14; the supersonic domain is located below curve 8. In case of supersonic flow around the cone the drag coefficient C_x equals the pressure coefficient C_p at $\sigma=0$ (see chapter 2).
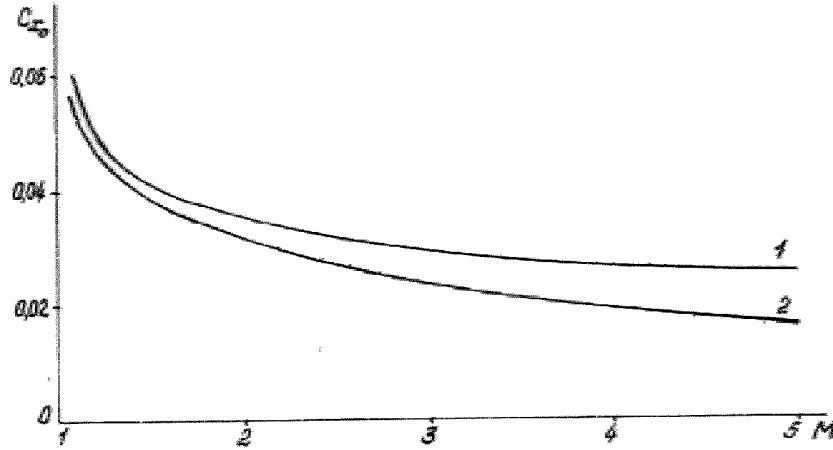

Fig. 16 Dependence of C_{xo} on M for the cone $\alpha=5°$; curve 1 corresponds to numerical calculation; curve 2 corresponds to calculation from formula (2.10)

Let us compare the drag coefficient of the cones at $\sigma=0$ ($C_{xo}=C_p$) obtained in this chapter with the ones calculated based on the slender body theory (2.10). In Fig. 16 and Fig. 17 the dependences $C_{xo}(M)$ are shown for the cones $\alpha=5°$ and $\alpha=10°$ respectively. Curve 1 corresponds to the values of C_{xo} obtained in this chapter, curve 2 corresponds to the values of C_{xo} calculated by formula (2.10).
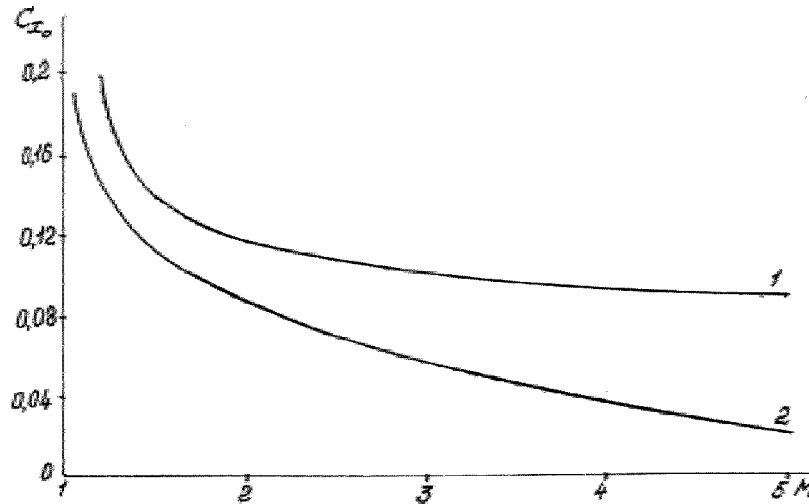

Fig. 17   Dependence of C_{xo} on M for the cone $\alpha=10°$; curve 1 corresponds to numerical calculation; curve 2 corresponds to calculation from formula (2.10)

From Fig. 16 it follows that for the cone $\alpha=5°$ the results of the numerical calculation obtained by formulas (6.1)-(6.6) are close to the results obtained by formula (2.10) at the Mach numbers $1.1 \leq M \leq 3$. This conclusion agrees with Fig. 14 which shows that the bow shock for the cone $\alpha=5°$ is close to the Mach line.

From Fig. 17 we can see the significant discrepancy between the values of C_{xo} calculated by formulas (6.1)-(6.6) and the ones calculated by formula (2.10). We cannot consider the cone $\alpha=10°$ to be a slender body in supersonic water flow. The numerical calculation shows (Fig. 14, 15) that at the Mach numbers on the interval $1<M<1.2$ this cone has a detached shock and the velocity on the cone surface exceeds the speed of sound if the Mach number is greater than 1.46. This flow is not described by the small perturbation theory. The third peculiarity of the slender body theory application to the supersonic cavitation flow is restriction of its results. For the drag coefficient of thin cone-cavitators this theory provides the exact values if the cone apex half-angle does not exceed 5°.

7. The comparison of the theoretical results with the experimental data

In the experimental works [26, 27, 28] the cavitation flows formed at the high speed body motion in water have been investigated on the Mach number interval $0.1 \leq M \leq 0.93$ (the body has a disk-cavitator). From the treatment of the experimental data we can conclude that in subsonic flow on the whole range of the Mach numbers the cavity is symmetrical with respect to the mid-section and the cavity profile is close to an ellipsoid of revolution. This conclusion agrees with the author's results obtained with the help of the slender body theory and the numerical methods. In Fig. 18 the continuous curve represents an ellipsoid of revolution; the points correspond to the experimental data [28] obtained on the Mach number interval $0.3 \leq M \leq 0.93$; the cavitation numbers have the order $10^{-4} \div 10^{-3}$.
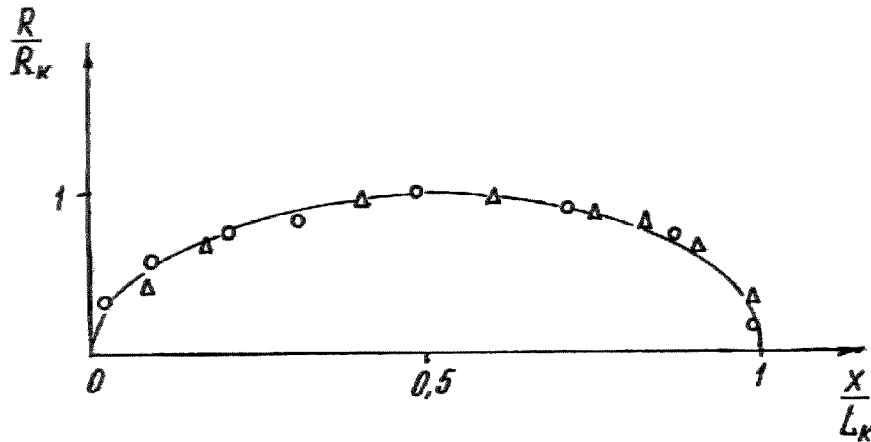

Fig. 18   Cavity profile; the continuous curve corresponds to an ellipsoid of revolution, the points correspond to the experimental data [28]

In [26, 27] the experimental values of the cavity dimensions obtained on the Mach number interval $0.1 \leq M \leq 0.7$ and the cavitation number interval $10^{-4} < \sigma < 10^{-2}$ have been compared with the asymptotic dependences at $\sigma \to 0$ [29]. The asymptotic formulas for the cavity mid-section radius and the cavity length scaled by the disk radius are written as follows [29]

$$R_k = \sqrt{\frac{C_x}{\sigma}}, \quad L_k = \frac{2}{\sigma}\sqrt{C_x \ln \frac{1}{\sigma}} \qquad (7.1)$$

In Fig. 19 the continuous curve represents the asymptotic dependence of the mid-section radius on the cavitation number (7.1); points 1 correspond to the experimental data [26, 27] (the Mach numbers are marked above the abscissa axis); points 2 correspond to the author's calculations [20].
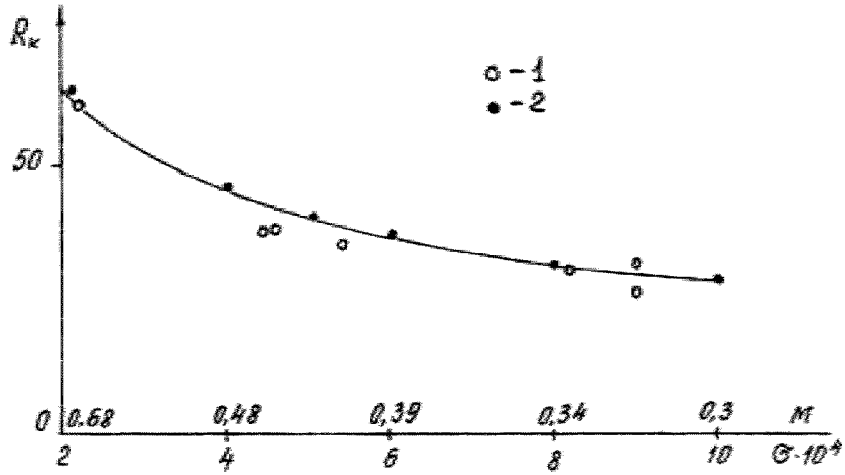
Fig. 19 Dependence of R_k on σ; the continuous curve corresponds to dependence (7.1); points 1 correspond to the experimental data [26, 27]; points 2 correspond to calculations [20]

In Fig. 20 the continuous curve represents the asymptotic dependence of the cavity length on the cavitation number (7.1); points 1 correspond to the experimental data [26, 27]; points 2 correspond to the author's calculations [20].
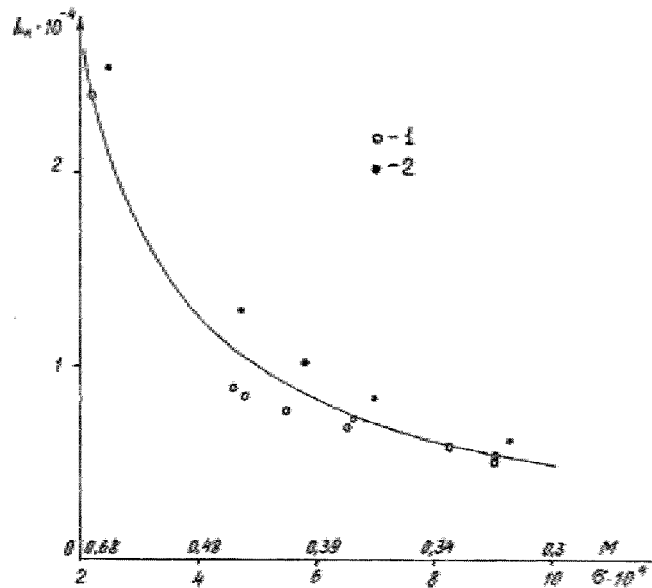

Fig. 20 Dependence of L_k on σ; the continuous curve corresponds to dependence (7.1); points 1 correspond to the experimental data [26, 27]; points 2 correspond to calculations [20]

From the examination of Fig. 18-20 we can conclude that the theoretical results agree with the experimental data.

In the United States and in the Institute of Hydromechanics (Ukraine) the tests are being carried out on the supersonic body motion in water. The quantitative experimental data are not presented, however, in 1998 a photograph of supersonic cavitation flow with a detached shock was published [30]. Also, the announcement was made in [30] that in the United States on July 17, 1997 the underwater

speed record was set (for the first time in water the speed of a body exceeds the speed of sound). The contour of the shock on the photograph shows that the Mach number is equal to 1.1 (or the speed of a body exceeds 1600m/s). In general, the image of the flow on the photograph corresponds to the author's theoretical result for the Mach number equal to 1.1 (Fig. 9).

Conclusions

The high speed cavitation flow in water has some peculiarities. The cavity has remarkable characteristics; it promotes not only the motion in water with small drag but also screens the body from shocks. On the cavity surface the constant velocity and the constant pressure conditions are satisfied, consequently the shocks are absent. The bow shock forms before the cavitator or on its apex (in case of thin cones), in the domain of cavity closure the trailing shock forms. For this scheme of flow the sharp change of the flow parameters does not take place on the transonic velocity range ($0.7 < M < 1.2$). As distinct from water, in air on the transonic velocity range the shocks form on the body surface and aerodynamic characteristics of body change considerably. In water on the transonic velocity range the parameters of the cavitation flow change smoothly as the Mach number increases. The passing though the speed of sound does not result in a substantial variation in the cavity shape as compared with subsonic flow. In spite of the small asymmetry of the shape about the mid-section the cavity shape in supersonic flow is close to an ellipsoid of revolution as it was before.

Water is rather law-compressible fluid as compared with air. In water many physical effects tied up with compressibility essentially differ from those in air. We can assume that the normal shock in water is isentropic and the flows are potential at the Mach numbers on the interval $1 < M \leq 2.2$. At the same Mach numbers the ratio of densities ρ_1/ρ_0 on the shock front in water is far less than that in air. As a result the distance between the forward shock and the cavitator surface in water is much greater than in case of continuous supersonic air flow. In supersonic water flow past a wedge or a cone the critical angles are significantly less than those in an air flow past the same bodies. The flow turning angle for the Prandtl-Meyer stream in water is far less than that in air at the same Mach numbers. All the factors mentioned above (the small losses of mechanical energy in the shocks, the considerable distance between the forward shock and the cavitator surface, the small deflection of flow in the stream about the cavitator edge) weakly prevent from the cavity expansion. In supersonic flow at the Mach numbers on the interval $1 \leq M \leq 1.4$ we do not observe the considerable narrowing and change of the cavity shape as compared with subsonic flow. The cavity expands in accordance with the law of conservation of energy in a liquid.

The slender body theory has a limited application for the investigation of the supersonic cavitation flows. First of all, in case of the thin cone-cavitators the solution obtained for the whole area of the flow is not valid for the flow past the cone edge. In the supersonic flow the Prandtl-Meyer stream forms at the edge. The stream must turn at the angle that is dependent upon the pressure within the cavity or the cavitation number. The incline of free stream line is less than the cone apex half-angle. It is impossible to satisfy this condition within the limits of the slender body theory. Secondly, for the outer solution the search for the second approximation to the cavity shape went beyond the limits of the slender body theory. In fact, the first approximation (an ellipsoid of revolution) is not a slender body in the front part where the shock forms. The shock is not described by the small perturbation theory. Thirdly, for the drag coefficient of thin cone-cavitators this theory provides the exact results if the cone apex half-angle does not exceed $5°$.

As distinct from the supersonic flow the slender body theory is more applicable for investigation on subsonic water flow. For example, the author has determined the cavitation parameters in subsonic flow around thin cones with apex half-angle equal to $5°$, $10°$ and $15°$. These results satisfy the momentum conservation law and for the particular case of incompressible fluid ($M=0$) agree with the numerical calculations. For the case when the parameter of the cavity thinness is far less than the parameter of the cavitator thinness the outer solution was found for subsonic flow. The comparison between the results of outer solution and the results of numerical calculation has shown good agreement.

References

1. Gurevich M. I., "Half-Body with Finite Drag in Subsonic Flow", Tr.TsAGI, #653, 1947, pp 1-12. (in Russian)

2. Yakimov Yu. L., "Asymptotic Laws of Degeneration of Thin Cavity Shapes", Izv. Akad. Nauk SSSR, Mekh. Zhidk. Gaza, #3, 1981, pp 3-10. (reprinted in the USA)

3. Yakimov Yu. L., "Thin Cavitation Cavity in a Compressible Fluid", in Problems of Contemporary Mechanics, Pt.1, Moscow University Press, Moscow, 1983, pp 63-73. (in Russian)

4. Vasin A. D., "Thin Axisymmetric Cavities in Subsonic Compressible Flow", Izv. Akad. Nauk SSSR, Mekh. Zhidk. Gaza, #5, 1987, pp 174-177. (reprinted in the USA)

5. Vasin A. D., "Thin Axisymmetric Cavities in Supersonic Flow", Izv. Akad. Nauk SSSR, Mekh. Zhidk. Gaza, #1, 1989, pp 179-181. (reprinted in the USA)

6. Serebryakov V. V., "Asymptotic Solutions of Problems of Axisymmetrical Supercavitation Flow in Slender Body Approximation", in Hydrodynamics of High Speeds, Chuvash. University Press, Cheboksari, 1990, pp 99-111. (in Russian)

7. Serebryakov V. V., "Asymptotic Solutions of Axisymmetrical Problems of Subsonic and Supersonic Separated Water Flows with Zero Cavitation Numbers", Dokl. Akad. Nauk Ukraine, #9, 1992, pp 66-71 (in Russian)

8. Al'ev G. A., "Separated Transonic Water Flow past a Circular Cone", Izv. Akad. Nauk SSSR, Mekh. Zhidk. Gaza, #2, 1983, pp 152-154. (reprinted in the USA)

9. Nishiyama T. and Khan O. F., "Compressibility Effects on Cavitation in High Speed Liquid Flow (Second report – transonic and supersonic liquid flows)", Bull. JSME, v. 24, #190, 1981, pp 655-661.

10. Zigangareeva L. M. and Kiselev O. M., "Calculation of the Compressible Subsonic Cavitation Flow past a Circular Cone", Prikl. Mat. Mekh., v.58, #4, 1994, pp.93-107. (reprinted in the USA)

11. Vasin A. D., "Calculation of Axisymmetric Cavities Downstream of a Disk in Subsonic Compressible Fluid Flow", Izv. Rus. Akad. Nauk, Mekh. Zhidk. Gaza, #2, 1996, pp 94-103. (reprinted in the USA)

12. Vasin A. D., "Calculation of Axisymmetric Cavities Downstream of a Disk in Supersonic Flow", Izv. Rus. Akad. Nauk, Mekh. Zhidk. Gaza, #4, 1997, pp 54-62. (reprinted in the USA)

13. Vasin A. D., "Application of the Slender Body Theory to Investigate Developed Axisymmetric Cavitation Flows in a Subsonic Stream of Compressible Fluid", Applied hydromechanics, Kiev, v.2 (74), #3, 2000, pp 17-25. (in Russian)

14. Logvinovich G. V., "Hydrodynamics of Flows with Free Boundaries", Naukova Dumka, Kiev, 1969, 215 p. (in Russian)

15. Guzevskii L. G., "Plane and Axisymmetric Problems of Hydrodynamics with Free Surface", Dissertation for a doctor's degree, Institute of Thermal Physics, Siberian Branch of the USSR Academy of Sciences, Novosibirsk, 1987, 300 p. (in Russian).

16. Liepmann H. W. and Roshko A., "Elements of Gasdynamics", John Wiley & Sons, Inc., New York, 1957.

17. Ashley H. and Landahl M. "Aerodynamics of Wings and Bodies", Addison-Wesley Publishing Com., Inc., Massachusetts, 1966.

18. Fletcher C. A. J., "Computational Techniques for Fluid Dynamics", Springer Verlag, Berlin et al., 1988.

19. Zamyshlyaev B. V. and Yakovlev Yu. S., "Dynamic Loads in Underwater Explosions", Sudostroenie, Leningrad, 1967, 387 p. (in Russian)

20. Vasin A. D., "Problems of Hydrodynamics and Hydroelasticity at High Speed Body Motion in Water", Dissertation for a doctor's degree, TsAGI, Moscow, 1999, 282 p. (in Russian)

21. Holst T. L. and Ballhaus W. F., "Fast, Conservative Schemes for the Full Potential Equation Applied to Transonic Flows", AIAA Journal, v. 17, #2, 1979, pp 145-152.

22. Loitsyanskii L. G., "Mechanics of Liquids and Gases", Pergamon Press, Oxford, 1966.

23. Cole R. H., "Underwater Explosions", University Press, Princeton, 1948.

24. Vasin A. D., "High-Speed Body Motion in Compressible Fluid", in Proceedings of the Scientific Meeting on High-Speed Hydrodynamics and Supercavitation, Laboratoire des Ecoulements Geophysiques et Industriels, Grenoble, France, 2000.

25. Vasin A. D., "Shocks and Conical Flows in a Supersonic Water Stream", Izv. Rus. Akad. Nauk, Mekh. Zhidk. Gaza, #5, 1998, pp 196-199 (reprinted in the USA)

26. Savchenko Yu. N., Semenenko V. N. and Serebryakov V. V., "Experimental Check of Asymptotic Formulas for Axisymmetric Cavities at $\sigma \to 0$", in Problems of High-Speed Hydrodynamics, Chuvash. University Press, Cheboksari, 1993, pp 117-122. (in Russian)

27. Savchenko Yu. N., Semenenko V. N. and Serebryakov V. V., "Experimental Investigation of Developed Cavitating Flows at Subsonic Flow Velocities", Dokl. Akad. Nauk Ukraine, #2, 1993, pp 64-69. (in Russian)

28. Savchenko Yu. N., "Investigation of High-Speed Supercavitating Underwater Motion of Bodies", in "High-Speed Body Motion in Water", AGARD-R-827, 1998, Reference 20.

29. Garabedian P. R., "The Calculation of Axially Symmetric Cavities and Jets", Pacific J. Math., #6, 1956, pp 611-689.

30. Kirchner I. N., "Supercavitating Projectile Experiments at Supersonic Speeds", Abstract, in "High-Speed Body Motion in Water", AGARD-R-827, 1998, Reference 35.